# Selenium reduction on Ni–Fe bimetallic nanoparticles: effect of process variables on reaction rates

Gautham B. Jegadeesan[a,*], Shashi B. Lalvani[b]

[a]*Department of Chemical Engineering, School of Chemical and Biotechnology, SASTRA University, Thirumalaisamudram, Thanjavur, India 613401, Tel. +91-9790947504; email: jegadeesan@scbt.sastra.edu*
[b]*Department of Paper and Chemical Engineering, Miami University, 64 D Engineering Building, 650 E. High St., Oxford, OH 45056, USA, Tel. 513-529-0763; email: lalvansb@miamioh.edu*

### a b s t r a c t

The use of bimetallic nanoparticles (BNPs) for contaminant reduction has gained prominence in recent years. In this work, the effect of initial selenium concentration, BNP loading, dissolved oxygen and pH on selenium reduction using Ni–Fe BNPs was investigated in batch kinetic and equilibrium studies. Equilibrium studies revealed that maximum selenium uptake was obtained at near neutral pH. Reaction kinetics of Se(VI) and Se(IV) reduction on Ni–Fe BNPs was best described Langmuir–Hinshelwood kinetics, with first order at low Se concentrations and zero order at high Se concentrations. For both selenium species, complete removal was obtained within 1 h of contact time. Reaction rates for Se(VI) were higher than that of Se(IV), indicating a two-step reduction process. With increase in Ni–Fe loading (i.e., increase in number of active surface sites), reaction rates also increased linearly, suggestive of an adsorption-controlled rate-limiting step. Deviation from linearity was observed due to the deactivation of the Ni–Fe catalysts. The presence of dissolved oxygen did not significantly affect Se reduction rates. Reduction of selenate, Se(VI), and selenite, Se(IV), on Ni–Fe BNPs occurred primarily due to: (1) adsorption of Se species on the active surface sites; (2) chemical reduction reactions on the surface and (3) sorption of the reduced Se species.

*Keywords:* Ni–Fe nanoparticles; Selenium; Reduction; Sorption; Catalytic activity

## 1. Introduction

The use of bimetallic nanoparticles (BNPs) for the treatment of groundwater and surface water contaminants has increased significantly in recent years [1–3]. In most BNPs, zerovalent iron ($Fe^0$) is the base metal, and the second transition metals (e.g., Ni, Cu, Co, Pd) or alkaline earth metal (e.g., Mg) is galvanically coupled with the base metal [4–15]. In comparison with $Fe^0$ nanoparticles (NPs) alone, BNPs have shown significant improvement in the treatment and remediation of several chlorinated hydrocarbons [5–9], polychlorinated biphenyls [10,11], and redox sensitive toxins like arsenic, selen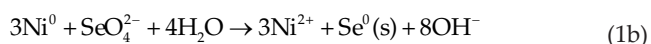ium and chromium [4,5,12–15]. The rate of contaminant removal (either via reduction or adsorption) using BNPs was found to be at least twofold higher compared with $Fe^0$ [4,5,9–15].

The increased efficiency with the use of BNPs is largely due to: (1) their high reactivity attributable to high surface areas and (2) the catalytic activity of the second metal when coupled with the base metal (i.e., $Fe^0$) [4,5,9–15]. First, the high specific surface areas of NPs, e.g., $Fe^0$ (33.5 $m^2\ g^{-1}$), compared with that of conventional microscale iron (typically of size <1 $m^2\ g^{-1}$) lead to higher rates of surface reactions [16]. With particle dimensions approaching nanometer sizes (5–10 nm), quantum effects begin to influence the physical and chemical properties [16]. These quantum effects cause changes in the Fermi level and band gap, which can lead

---

\* Corresponding author.

to increases in reactivity with decreasing particle size [16]. Second, when a second metal is galvanically coupled with base metal, the more noble metal participates in the reaction, while other metal corrodes to galvanically protect the noble metal. This galvanic coupling of two metals: (1) increases the catalytic activity of the BNPs; (2) retards the formation of the oxide film on the surface of base metal via an in situ regeneration process; and (3) induces the less nobler metal to release electrons at a faster rate thereby enhancing the rate of contaminant removal [4,5,9–15]. Finally, the ability of the metal oxides formed after oxidation of the bimetals to adsorb the contaminant and any intermediates (formed during reduction reactions) augments contaminant removal [4,5,9–15].

In our previous work [4], we reported the use of Ni–Fe BNPs for the reduction of selenate, Se(VI), from aqueous solutions. The rate of selenate reduction on Ni–Fe BNPs was 3–4 times higher when compared with $Fe^0$. The standard reduction potential ($E^0$) for Fe and Ni are –0.44 V and –0.28 V, respectively, suggesting that the spontaneous oxidation of the metals is thermodynamically favored. The mechanism proposed for Se(VI) reduction was as follows: (1) reduction of Se(VI) on the $Ni^0$ surface, resulting in the oxidation of $Ni^0$ to $Ni^{2+}$ (reaction (1a) or (1b)); (2) oxidation of galvanically coupled $Fe^0$, thereby releasing its electrons for the regeneration of Ni (reactions (2) and (3)); and (3) formation of metal oxides that would subsequently adsorb/complex reduced Se species (i.e., Se(IV) or $Se^0$) (reaction (4)).

$$Ni^0 + SeO_4^{2-} + H_2O \rightarrow Ni^{2+} + SeO_3^{2-} + 2OH^- \tag{1a}$$

$$3Ni^0 + SeO_4^{2-} + 4H_2O \rightarrow 3Ni^{2+} + Se^0(s) + 8OH^- \tag{1b}$$

$$Fe^0 \rightarrow Fe^{2+} + 2e^- \tag{2}$$

$$Ni^{2+} + 2e^- \rightarrow Ni^0_{(s)} \tag{3}$$

$$Fe^{2+} + 2OH^- \rightarrow Fe(OH)_2 \text{ or } FeOOH \tag{4}$$

Reduction of Se(VI) or Se(IV), either via a mechanism of stepwise reduction to Se(IV) and then finally to $Se^0$ or Se(–II) or via a direct reduction to $Se^0$, depends on the formal cell potential of the metallic powder. X-ray photoelectron spectroscopy and scanning transmission electron microscopy (STEM) based X-ray energy-dispersive spectroscopy (XEDS) analysis of Se(VI) and Se(IV) reduction on $Fe^0$ NPs strongly indicated that the final reduced forms of Se were selenide (Se(–II)) and elemental selenium ($Se^0$) [13,14]. Stepwise reduction of Se(VI) was suggested, and the presence of $Fe^{2+}$ oxides coat over the $Fe^0$ shell encapsulated the reduced selenium forms [13,14]. Rates of BNP catalytic reactions depend on several factors such as structural properties of BNPs; contaminant concentration; reaction conditions such as pH, presence or absence of dissolved oxygen; and impurities on the catalytic surface. Certain reaction conditions such as contaminant concentration and temperature will increase reaction rates, while

absence of oxygen may reduce rates [4,12–17]. As noted in the mechanism above, spontaneous oxidation of the metals, while inducing reduction reactions, also results in the formation of an oxide film on the surface of NPs. The presence of the oxide layer can deactivate the BNP surface, since the zerovalent metal on the surface is no longer available for reaction (corrosion, reduction or adsorption). BNPs undergo rapid deactivation due to the formation of iron oxide, which engulfs the matrix within 24 h [2–4]. Greenlee et al. [17] noted that presence of oxygenated conditions enhanced oxidation rates of $Fe^0$ NPs, resulting in the formation of metal oxides on the NP core. However, Schrick et al. [8] noted in their study that Ni–Fe BNPs retained their activity for longer durations.

A crucial understanding of the various factors influencing selenium reduction is warranted for assessing feasibility in field applications. In this present work, we report the effect of reaction conditions, i.e., pH, initial Se concentration, BNP loading, and dissolved oxygen on the selenium reduction rates. The effect of pH was determined in equilibrium studies. Kinetic data was collected to determine the effect of select parameters on reaction rates. In addition, the loss of catalytic activity of the Ni–Fe BNPs upon use was also determined.

## 2. Materials and methods

### 2.1. Materials

Sodium selenite ($Na_2SeO_3$), sodium selenate ($Na_2SeO_4$), hydrochloric acid (HCl), sodium hydroxide (NaOH), ferric chloride ($FeCl_2.7H_2O$), nickel chloride, anhydrous ($NiCl_2$) and sodium borohydride ($NaBH_4$) were obtained from Fischer Scientific (Chicago, USA) and used as received.

### 2.2. Synthesis of bimetallic Ni–Fe nanoparticles

Synthesis of Ni–Fe BNPs involves the simultaneous reduction of the metal ions in aqueous solution by $NaBH_4$ [4]. Equimolar metal salt solutions of (0.5 M) nickel and iron was treated with excess borohydride solution (0.8 M) and ultrasonically agitated for 30 min. Ultrasonic agitation of the mixture ensures small particle size of the Ni–Fe BNPs. The precipitated solids, i.e., Ni–Fe, were recovered via centrifugation, followed by drying at 85°C in nitrogen-rich atmosphere for 24 h, to prevent oxidation of iron or nickel.

### 2.3. Batch experiments on selenium reduction

Stock solutions (1,000 mg L$^{-1}$) of Se(IV) (7.87 mM) and Se(VI) (7 mM) were prepared in deionized water and maintained at near neutral pH (~7.0). Table 1 presents the summary of parameters investigated and the range of those parameters. Among the various parameters, pH has a strong influence on the rate of the reaction, since sorption of the contaminant on the surface determines surface reaction rates. Therefore, we initially performed equilibrium pH studies to determine the pH at which maximum sorption occurred. Equilibrium studies using different Se(VI) and Se(IV) concentrations at five different pH conditions were conducted. The solution pH was varied using 0.1 N HCl or 0.1 N NaOH. As detailed below, maximum Se(VI)

uptakes were observed at pH of 7.1. Therefore, subsequent experiments were performed at that pH value.

Se concentrations in groundwater and surface water range from 0.01 $\mu g\ L^{-1}$ to 1.8 mg $L^{-1}$ [18]. However, Se(IV) and Se(VI) reduction kinetics at such low concentration was observed to be very fast to collect usable kinetic data. Therefore, higher Se concentrations were used to determine the effect of reaction parameters on rates. The kinetics of most heterogeneous catalytic reactions depend on the concentration of the reactant and the catalyst loading. In this study, the initial selenium concentration was varied from 10 to 100 mg $L^{-1}$ in the study on the impact of initial Se concentration. Ni–Fe BNPs loading was varied from 0.25 to 5 mg $L^{-1}$. Since the reduction of Se using Ni–Fe BNPs is dependent on the oxidation of the metals, effect of dissolved oxygen on reaction rates was also investigated. The selenate solution was purged with $N_2$ gas to create anaerobic condition, and air to create aerobic conditions. The residence time for the reduction studies was about 3 h unless otherwise noted. The solution pH in all experiments except those in which the pH was controlled corresponds to the pH before the addition of solids to the flasks (pH = 7.0 ± 0.1). A small volume of the solution (less than 1 mL) was collected at desired intervals in Whatman Autovial syringeless filters (Fisher Scientific, Chicago) and then analyzed. For the kinetic studies, samples were collected at desired intervals and filtered for analysis.

## 2.4. Characterization and analysis

Total selenium was measured using an inductively coupled plasma–mass spectrometer (DWR Bryte Laboratory, California) using EPA Method 200.8. The detection limit was 10 $\mu g\ L^{-1}$. Selenium speciation analysis was performed using an ion chromatograph (DX-500, Dionex, California). The particle size distribution was obtained using a Laser Microtrac Particle Size Analyzer. Energy-dispersive X-ray (EDX) spectroscopy was utilized to quantify the relative content of each metal in the bimetallic particles. Quantachrome Nova 2000 BET analyzer was used to estimate the surface areas of the powders. The NP size and structure were analyzed using a Hitachi scanning electron microscope (SEM) and transmission electron microscope (TEM).

## 3. Results and discussion

### 3.1. Bimetallic nanoparticle characterization

Fig. 1 presents the representative SEM and TEM images of the Ni–Fe BNPs. Relative composition of the Ni–Fe BNPs as seen in the EDX analysis was 1:1 nickel:iron. Residual chloride was present in the Ni–Fe BNPs, an artifact of using nickel and ferric chloride for synthesis. SEM and TEM images showed that the most of the particles were submicron in size, and the average particle size obtained from the TEM was approximately 50 nm. The mean size of the BNPs ranged from 0.2 to 1 $\mu m$, due to agglomeration. The Brunauer–Emmett–Teller surface area was 45.1 $m^2\ g^{-1}$.

Table 1
Experimental conditions

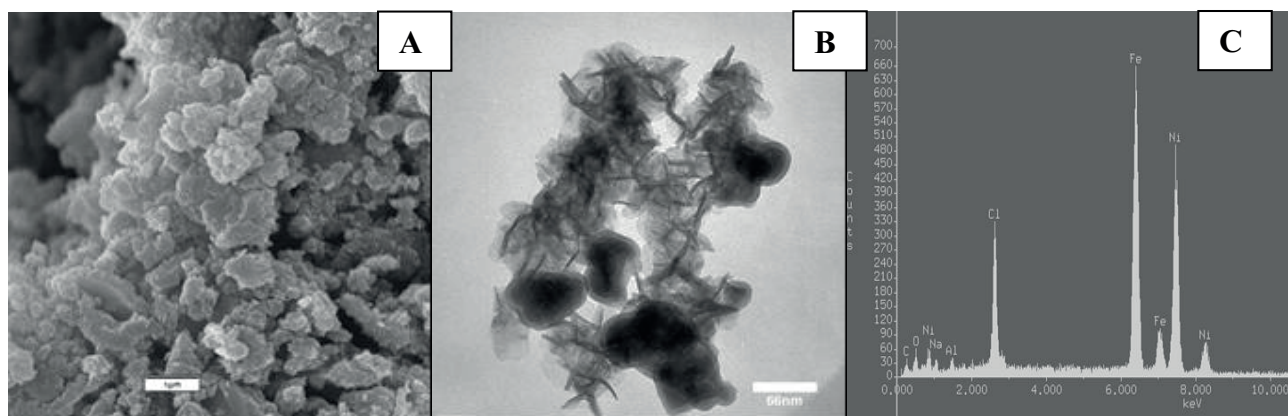| Range of parameter | Parameter investigated | | | | |
| --- | --- | --- | --- | --- | --- |
| | Initial Se(VI) concentration | Initial Se(IV) concentration | Ni–Fe loading | pH | Dissolved oxygen |
| Initial Se(VI) conc. (mg $L^{-1}$) | 10–100 | – | 1 | 10, 25, 50 | 50 |
| Initial Se(IV) conc. (mg $L^{-1}$) | – | 10–100 | 1 | 10, 25, 50 | 50 |
| Ni–Fe loading (g $L^{-1}$) | 5 | 5 | 0.5–5 | 5 | 5 |
| pH | 7.0 ± 0.1 | 7.0 ± 0.1 | 7.0 ± 0.1 | 2.9–10.5 | 7.0 ± 0.1 |
| Temperature (°C) | 25 | 25 | 25 | 25 | 25 |



Fig. 1. SEM (A), TEM (B) and EDX (C) analysis of the Ni-Fe BNPs.

### 3.2. Effect of pH

For catalytic reactions to occur, the reactant must attach itself to the surface of the catalyst either via adsorption or via complexation processes. Solution pH is one of the key parameters in Se(VI) removal, as it affects Se(VI) and Se(IV) adsorption capacities. Therefore, equilibrium–pH studies were performed to identify pH conditions that would ensure maximum Se(VI) reduction. Fig. 2 shows Se sorption vs. solution pH. The equilibration time was 72 h, at a BNP loading of 5 g L$^{-1}$. Selenium removal via sorption/reduction is maximum in neutral pH range and decreased beyond neutral pH. Percentage removals for Se(IV) were higher than Se(VI), expectedly. Studies have shown that Se(VI) forms weak outer-sphere complexes, while Se(IV) forms strong inner-sphere complexes with metal/metal oxides [19–22]. Su and Suarez [20] and Yoon et al. [22] observed maximum Se removal (via sorption) on Fe oxides and Fe$^0$ in the pH range of 4–7. Beyond pH of 8.0, Se sorption tends to decrease. Decrease in Se(VI) removal in highly acidic or basic conditions is largely due to: (1) competition for surface sites for Se(VI) reduction and hydrogen evolution at low pH (where H$^+$ concentration

are high) and (2) formation of metal oxides/oxyhydroxide precipitates at high pH, which act as a physical barrier to selenium reduction on the BNP surface.

Based upon the pH-sorption curves, an additional equilibrium study was performed to determine the adsorption constants. Sorption experiments at pH 3.6 and 7 were performed using Se concentration of 100 and 250 mg L$^{-1}$, respectively. Fig. 3 shows the Se(IV) and Se(VI) surface coverage vs. equilibrium Se concentration for the two pH conditions. The data was modeled using Langmuir isotherm equation (Table 2), assuming monolayer sorption and the maximum capacity of the Ni–Fe BNPs for Se sorption were determined. The plot of $1/q$ vs. $1/C_e$ was a straight line ($R^2 > 0.9$), and the maximum capacity was determined using the slope and intercepts. As seen in Table 2, the maximum capacity for Se(IV) and Se(VI) was 12–16 mg g$^{-1}$, consistent with Se sorption capacities reported elsewhere [4,19–22]. The sorption capacity of Se on Ni–Fe were similar, except for Se(VI) at neutral pH, which was almost twice the other capacities. Deviation from Langmuir isotherm model was noted at high equilibrium concentrations (corresponding to high initial Se concentration of 100
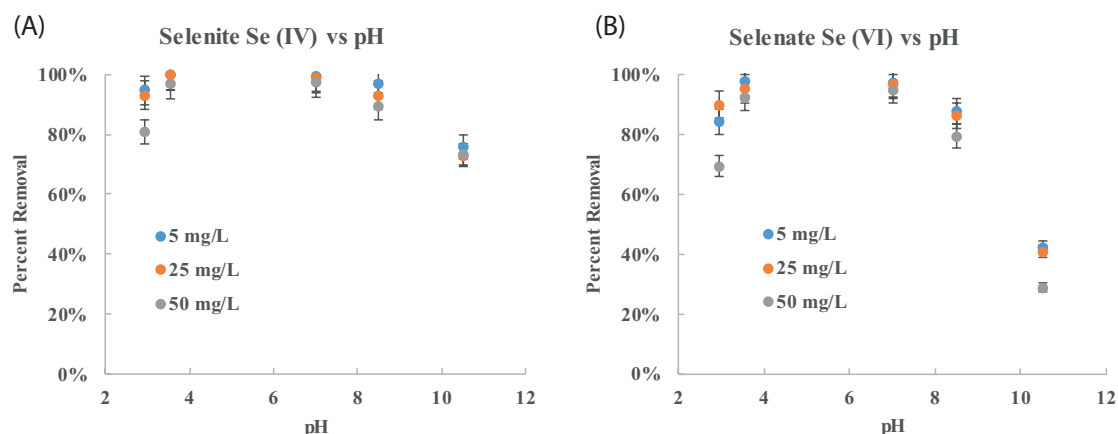


Fig. 2. Effect of pH on selenium removal at different Se(IV) (A) and Se(VI) (B) concentrations.
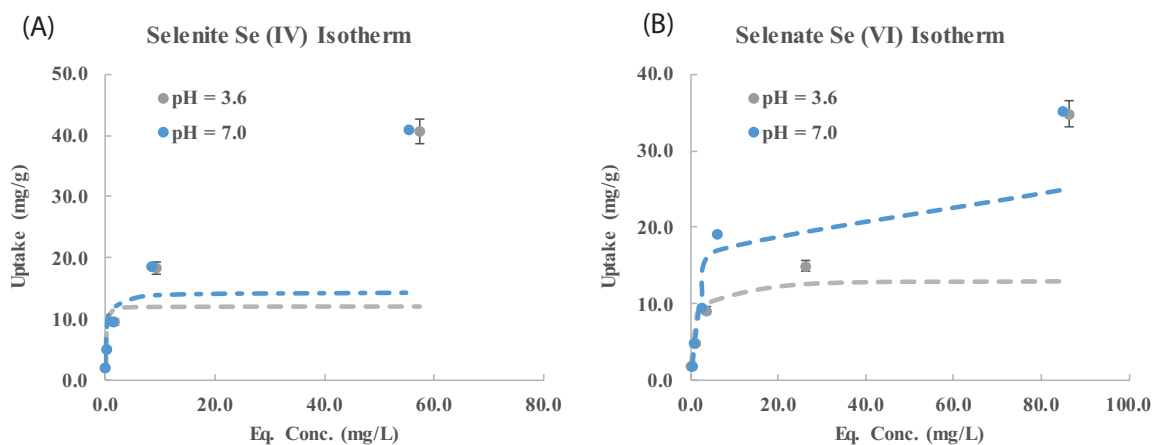


Fig. 3. Adsorption isotherms for Se(IV) (A) and Se(VI) (B) at two different pH conditions. Dashed lines show the modeled Langmuir isotherm.

and 250 mg L$^{-1}$). Langmuir isotherm model, which assumes monolayer and an intact surface, may not be the best descriptor of Se(VI) sorption on Ni–Fe, due to the series of redox reaction occurring on the Ni–Fe BNP surface. However, they have been used frequently to determine sorption capacities. At very high Se(VI) concentration, surface coverage are dependent on the number of active (reactive) sites available for sorption. The observed surface coverage was found to be significantly higher than the modeled data. This indicated that the more number of reactive sites (in addition to those present on the BNP surface) participated in the sorption process. XEDS–STEM studies on Se(IV) reduction on Fe$^0$ suggested that Fe$^0$ induced reduction process and the solid phase diffusion of Se(IV) and its reduced species into the inner core of Fe$^0$ were the predominant mechanisms [14]. The observed data here appeared to be in concurrence with mechanisms reported elsewhere [14]. Higher sorption uptakes (surface coverage) at pH of 7 is beneficial since natural pH of contaminated surface and groundwaters ranges between 6.5 and 8.5.

### 3.3. Effect of selenium concentration of rate kinetics

Fig. 4(A) presents the kinetic data for Se(IV) reduction on Ni–Fe BNPs, expressed as the ratio of concentration to

initial concentration ($C/C_0$). In general, Se(IV) concentration decreased exponentially with time. Near complete removal (non-detect concentration) was observed within 10 min of reaction, when 5 mg L$^{-1}$ was treated with 5 g L$^{-1}$ of Ni–Fe BNPs. As initial concentration increased from 10 to 50 mg L$^{-1}$, time required to achieve complete removal also increases, suggestive of decrease in reaction rates. It was observed that almost 98% of Se(IV) removal was obtained for initial Se(IV) concentrations of 10–50 mg L$^{-1}$. Fig. 4(B) presents the kinetic data for Se(VI) reduction on Ni–Fe BNPs, expressed as the ratio of concentration to initial concentration ($C/C_0$). As the initial concentration increased tenfold, the removal percentage decreased from 100% to almost 80% within 10 min of reaction time (final Se(VI) concentration = 9.4 mg L$^{-1}$). A comparison of Se(IV) and Se(VI) concentration-time plots clearly indicates that Se(IV) removal was faster when compared with Se(VI) removal.

Reduction of contaminants on heterogeneous catalytic surfaces is often expressed by Langmuir–Hinshelwood kinetics, shown in Eq. (A) [4,23,24]:

$$-\frac{dC_A}{dt} = \frac{k_s K_{eq} C_A}{1 + K_{eq} C_A} \tag{A}$$

In the above equation, $C_A$ is the contaminant (Se) concentration; $k_s$ is the surface reaction rate constant and $K_{eq}$ is the equilibrium constant. At very low reactant concentration ($C_A \ll 1$), the rate of reaction assumes first-order kinetics, and at high reactant concentrations, reaction follows zero-order kinetics. Studies on BNP-assisted dechlorination and other reduction reactions have indicated that the reaction of the adsorbed molecules on the catalyst surface is the rate-determining step, with all the other steps (adsorption and desorption) assumed to be in equilibrium [4,23,24]. Fitting the experimental data to the mathematical expressions from Langmuir–Hinshelwood kinetics has often shown significant deviations due to the following reasons: (1) adsorption of reactant on the catalyst is a function of the available active surface sites; therefore, pseudo-steady-state conditions may
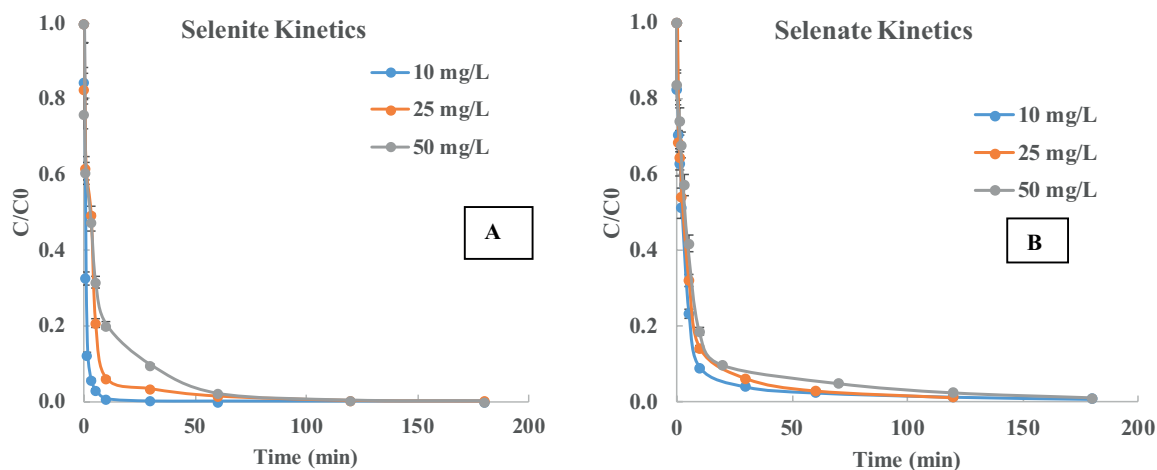
Table 2
Sorption capacity (mg g$^{-1}$) and sorption potential (L g$^{-1}$) obtained using Langmuir isotherms[a]

| Langmuir isotherm model[a] | | | | | |
|---|---|---|---|---|---|
| Se(IV) | | | Se(VI) | | |
| pH | Maximum capacity (mg g$^{-1}$) | Potential | pH | Maximum capacity (mg g$^{-1}$) | Potential |
| 3.6 | 12.2 | 0.9 | 3.6 | 13.2 | 19.02 |
| 7 | 14.4 | 0.32 | 7 | 25.8 | 3.15 |

[a]Langmuir equation: $q = \frac{aq_{max}C_e}{1 + aC_e}$, where $q$ = surface coverage; $q_{max}$ = maximum coverage (capacity); $C_e$ = equilibrium solute concentration and $a$ = adsorption potential.



Fig. 4. Kinetics of Se(IV) (A) and Se(VI) (B) reduction on Ni–Fe BNPs. Se concentration normalized to initial Se concentration, $C/C_0$.

not accurately represent the reaction kinetics, and (2) catalyst surface comprises both active and non-reactive sites, not accounted for in the models.

Kinetic studies revealed that both Se(IV) and Se(VI) followed Langmuir–Hinshelwood kinetics. The inverse of the reaction rate, ($-\frac{dt}{dC_A}$) increased linearly with $1/C_A$. The linear expression was fitted to the data, and the goodness of fit was 0.92–0.97. Table 3 shows the various rate constants ($k_s$ and $K_{eq}$). A common method used to distinguish whether a certain heterogeneous catalytic reaction is adsorption or surface reaction limited involves the measurement of the initial rate as a function of reactant concentration [21]. If the initial rate linearly increases with reactant concentration, it is adsorption controlled. If the increase is asymptotic, then it is surface reaction or desorption controlled. As can be seen in Table 3, the initial rate increased linearly with Se concentration for both Se(IV) and Se(VI). This suggested that both Se(IV) and Se(VI) reduction on Ni–Fe BNPs was adsorption controlled. The ratio of the $k_s$ to $K_{eq}$ was observed to be high, clearly indicating an adsorption-controlled process. The ratio was less pronounced for Se(IV), suggesting both adsorption and surface reaction mechanisms may control the reaction rate. The rate of Se(VI) reduction by Ni–Fe BNPs was higher than that for Se(IV), probably due to a two-electron requirement to reduce from Se(VI) to Se(IV) (less energy) as opposed to a four-electron reduction (Se(IV) to Se$^0$, higher energy). At the start of the reaction, the number of reactive sites on the BNP surface is higher, resulting in higher rates of surface catalyzed reaction. As reaction progress, the reduction of Se(IV) to its elemental state on the catalyst surface renders the sites inactive and lowers initial rates. Catalytic activity of the zerovalent metals decreases due to: (1) formation of metal oxides on the catalytic surface and (2) decreased porosity [13,14,25].

### 3.4. Effect of dissolved oxygen and catalyst loading

The chemical stability and longevity of Ni–Fe BNPs depends on rate of oxidation of the zerovalent metals in aqueous solutions. In the subsurface, anoxic conditions at high pH values (7.5–8.5) are often observed [14,17,25,26]. The presence or absence of dissolved oxygen in aquatic streams can affect Se removal on Ni–Fe BNPs in multiple ways. Higher levels of $O_2$ will increase metal oxidation rates, increasing the initial rates of reactions, at the expense of chemical stability or longevity of the BNPs. Conversely, negligible or lower levels of $O_2$ will impede the reaction rates, but the longevity of the BNPs will increase [25,26]. The dissolved oxygen concentration was measured to be <0.5 mg L$^{-1}$ for anoxic systems. When gases were not purged (i.e., natural systems), dissolved oxygen was measured to be 5 mg L$^{-1}$.

Fig. 5 shows the comparison of the kinetic data under aerobic and anaerobic conditions. It was observed that under oxygenated conditions, the black Ni–Fe BNPs turned brown faster, possibly suggesting a faster rate of oxide film

Table 3
Kinetic rate constant for Se(IV) and Se(VI)

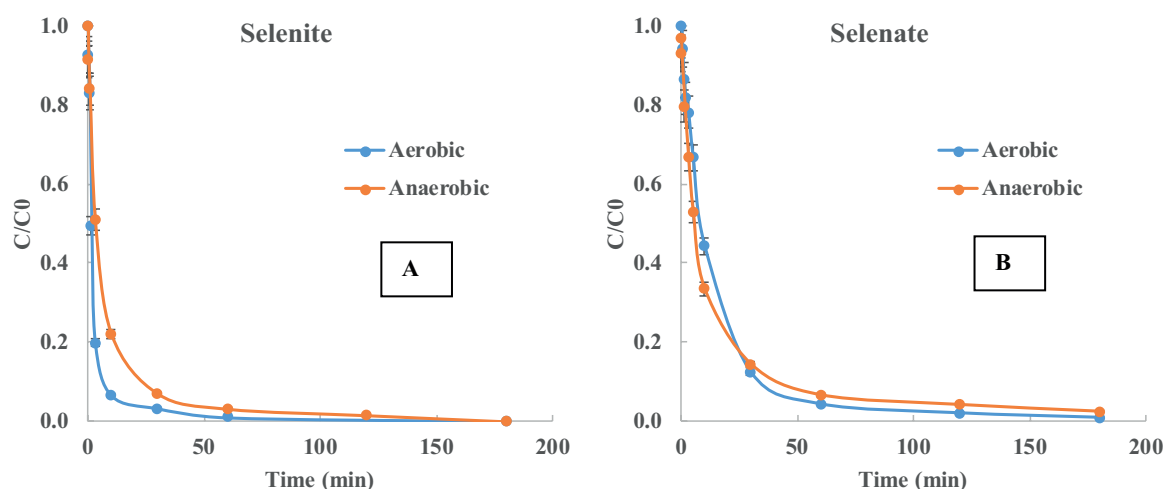| Concentration (mg L$^{-1}$) | Se(IV) | | | Se(VI) | | |
|---|---|---|---|---|---|---|
| | $k_s$ (mg L$^{-1}$ min$^{-1}$) | $K_{eq}$ (L mg$^{-1}$) | Initial rate | $k_s$ (mg L$^{-1}$ min$^{-1}$) | $K_{eq}$ (L mg$^{-1}$) | Initial rate |
| 10 | 5.291 | 0.133 | 52.91 | 61.3 | 0.1 | 613.5 |
| 25 | 2.564 | 0.118 | 64.10 | 41.7 | 1.0 | 1,041.7 |
| 50 | 1.67 | 0.09 | 83.33 | 32.3 | 0.4 | 1,612.9 |



Fig. 5. Reaction kinetics of Se(IV) (A) and Se(VI) (B) reduction under aerobic and anaerobic conditions.

generation, when compared with the Ni–Fe BNPs in deoxygenated conditions. However, the kinetic data in Fig. 5 shows no significant difference in the Se removal under the different conditions. The surface reaction rate constant ($k_s$) obtained from the kinetic data (using Eq. (A)) ranged from 10.3 to 12.7 mg L$^{-1}$ min$^{-1}$, suggesting that the surface reaction rate did not significantly change. It was observed that the rate of Se(VI) reduction was higher than rate of Se(IV) reduction in both conditions. Interestingly, the equilibrium constant ($K_{eq}$) was significantly low for Se(IV) (ranged from 3.4 to 4.4), when compared with Se(VI) (13.4–14.4), suggesting higher Se(VI) reduction and subsequent adsorption.

Increasing the catalyst loading (i.e., the number of active sites on the catalyst surface) is expected to increase reaction rate. The effect of Ni–Fe BNP loading on Se reduction kinetics is shown in Fig. 6. Since the activity of Ni–Fe BNPs reduced as time progressed, the duration of the kinetic experiments was limited to 10–30 min. Langmuir–Hinshelwood rate

expression was used to determine equilibrium and rate constants. The goodness of fit was 0.91–0.98, and the variation in rate constants with loading is presented in Fig. 7. The surface reaction rate decreased ($k_s$) with increasing loading, and the decrease for more pronounced for Se (VI), compared with Se(IV). However, the equilibrium constant increased, clearly suggesting that adsorption was the rate controlling step. With increase in the active site density, more Se was being adsorbed, and therefore, the equilibrium constant was higher.

## 4. Conclusions

To understand the effect of reaction parameters on Se(VI) reduction on Ni–Fe BNPs, batch kinetic and equilibrium experiments were performed. The effect of initial Se concentration, BNP loading, pH and dissolved oxygen was investigated. Selenium reduction was maximum at near neutral pH range (pH = 7.1), with decreased surface
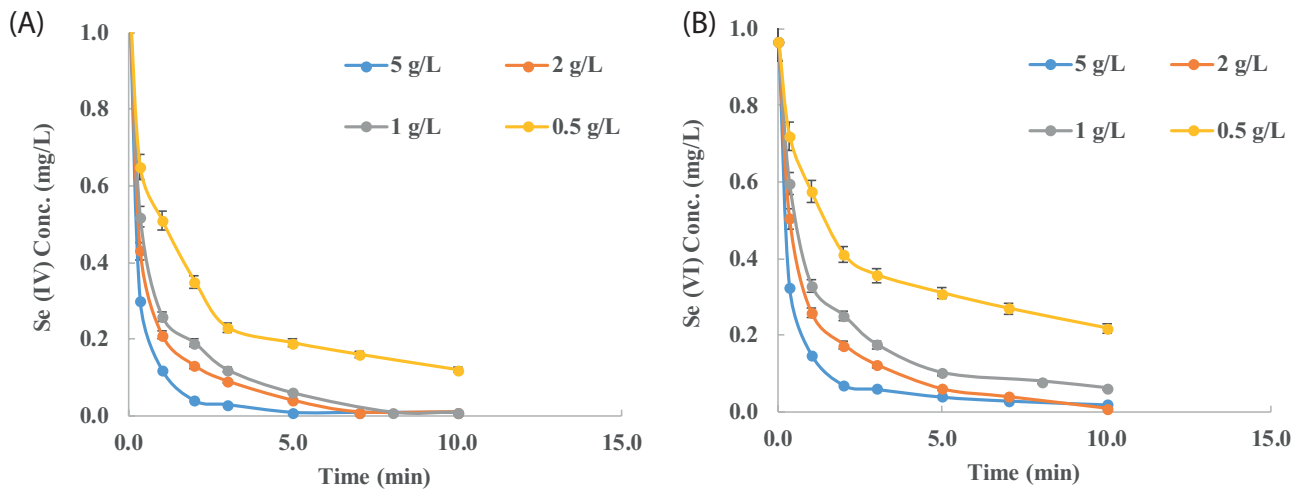


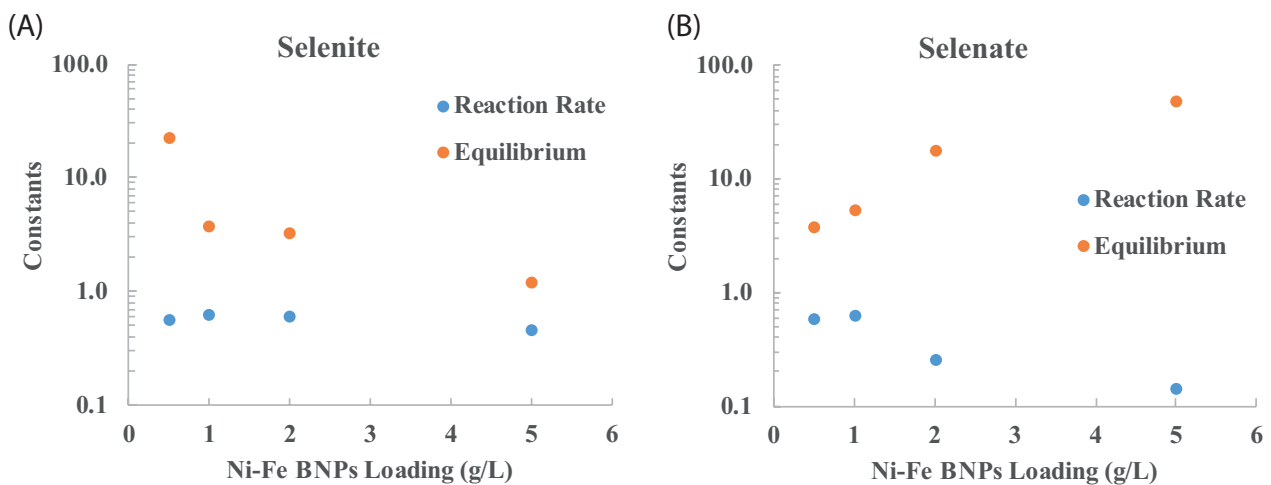Fig. 6. Kinetics of Se(IV) (A)and Se(VI) (B) reduction on Ni–Fe BNPs at various solid loadings.



Fig. 7. Effect of Ni–Fe BNP loading on reaction rate constants for Se(IV) (A) and Se(VI) (B).

coverage at either ends of the pH spectrum. Competition for active sites by protons or deactivation of surface sites due to formation of iron oxyhydroxides may be reasons for low coverage at low and high pH, respectively. Deviation from assumed monolayer adsorption was observed. Se(IV) was more rapidly removed and had higher removal efficiency, when compared with Se(VI) removal. Initial reaction rates increased with Se concentration, indicating adsorption controlled rate-limiting step. Overall, the rate of reaction followed Langmuir–Hinshelwood kinetics, with first order at low Se concentration, shifting to zero order at high concentration. The amount of Ni–Fe BNPs used significantly affected rates of reduction, with greater dependence on number of active surface sites at high Se concentration. Rate constants increased linearly with the number of active sites, with deviation observed at very high loadings. It was observed that the presence or absence of oxygen did not significantly impact Se removal. Decrease in reaction rate with increasing time was attributed to loss of catalytic activity of the Ni–Fe catalyst. The study concludes that Ni–Fe BNPs are efficient catalysts for the reduction of oxyanionic trace metals such as selenium, both in surface and groundwater.

## References

[1] B. Karn, T. Kuiken, M. Otto, Nanotechnology and in situ remediation: a review of the benefits and potential risks, Environ. Health Perspect., 117 (2009) 1823–1831.

[2] D. Caroll, B. Sleep, M. Krol, H. Boparai, C. Kocur, Nanoscale zerovalent iron and bimetallic particles for contaminated site remediation, Adv. Water Res., 51 (2013) 104–122.

[3] W.J. Liu, T.T. Qian, H. Jiang, Bimetallic Fe nanoparticles: recent advances in synthesis and application in catalytic elimination of environmental pollutants, Chem. Eng. J., 236 (2014) 448–463.

[4] K. Mondal, G. Jegadeesan, S.B. Lalvani, Removal of selenate by Fe and NiFe nanosized particles, Ind. Eng. Chem. Res., 43 (2004) 4922–4934.

[5] D.W. Elliott, W-x. Zhang, Field assessment of nanoscale bimetallic particles for groundwater treatment, Environ. Sci. Technol., 35 (2001) 4922–4926.

[6] M.O. Nutt, J.B. Hughes, M.S. Wong, Designing Pd-on-Au bimetallic nanoparticle catalysts for trichloroethene hydrodechlorination, Environ. Sci. Technol., 39 (2005) 1346–1353.

[7] W.X. Zhang, C.B. Wang, H.L. Lien, Treatment of chlorinated organic contaminants with nanoscale bimetallic particles, Catal. Today, 40 (1998) 387–395.

[8] B. Schrick, J.L. Blough, A.D. Jones, T.E. Mallouk, Hydrodechlorination of trichloroethylene to hydrocarbons using bimetallic nickel–iron nanoparticles, Chem. Mater., 14 (2002) 5140–5147.

[9] A. Colombo, C. Dragonetti, M. Magni, D. Roberto, Degradation of toxic halogenated organic compounds by iron-containing mono-, bi-and tri-metallic particles in water, Inorg. Chim. Acta, 431 (2015) 48–60.

[10] Z. Zhang, S. Hu, S.A. Baig, J. Tang, X. Xu, Catalytic dechlorination of Aroclor 1242 by Ni/Fe bimetallic nanoparticles, J. Colloid Interface Sci., 385 (2012) 160–165.

[11] H. Choi, S. Agarwal, S.R. Al-Abed, Adsorption and simultaneous dechlorination of PCBs on GAC/Fe/Pd: mechanistic aspects and reactive capping barrier concept, Environ. Sci. Technol., 43 (2009) 488–493.

[12] G. Jegadeesan, K. Mondal, S.B. Lalvani, Arsenate remediation using nanosized modified zerovalent iron particles, Environ. Prog. Sustain. Energy, 24 (2005) 289–296.

[13] L. Ling, B. Pan, W-x. Zhang, Removal of selenium from water with nanoscale zero-valent iron: mechanisms of intra-particle reduction of Se (IV), Water Res., 71 (2015) 274–281.

[14] C. Tang, Y.H. Huang, Z.H. Zhang, Reductive removal of selenate by zero-valent iron: the roles of aqueous $Fe^{2+}$ and corrosion products, and selenate removal mechanisms, Water Res., 67 (2014) 166–174.

[15] S. Zhou, Y. Li, J. Chen, Z. Liu, Z. Wang, P. Na, Enhanced Cr(VI) removal from aqueous solutions using Ni/Fe bimetallic nanoparticles: characterization, kinetics and mechanism, RSC Adv., 4 (2014) 50699–50707.

[16] C.T. Campbell, S.C. Parker, The effect of size-dependent nanoparticle energetics on catalyst sintering, Science, 298 (2002) 811–814.

[17] L.F. Greenlee, J.D. Torrey, R.L. Amaro, J.M. Shaw, Kinetics of zero valent iron nanoparticle oxidation in oxygenated water, Environ. Sci. Technol., 46 (2012) 12913–12920.

[18] J.E. Conde, M. Sanz Alaejos, Selenium concentrations in natural and environmental waters, Chem. Rev., 97 (1997) 1979–2003.

[19] L. Liang, W. Yang, X. Guan, J. Li, Z. Xu, J. Wu, Y. Huang, X. Zhang, Kinetics and mechanisms of pH-dependent selenite removal by zero valent iron, Water Res., 47 (2013) 5846–5855.

[20] C.M. Su, D.L. Suarez, Selenate and selenite sorption on iron oxides: an infrared and electrophoretic study, Soil Sci. Soc. Am. J., 64 (2000) 101–111.

[21] J.T. Olegario, N. Yee, M. Miller, J. Sczepaniak, B. Manning, Reduction of Se(VI) to Se(-II) by zerovalent iron nanoparticle suspensions, J. Nanopart. Res., 12 (2010) 2057–2068.

[22] I.H. Yoon, K.W. Kim, S. Bang, M.G. Kim, Reduction and adsorption mechanisms of selenate by zero-valent iron and related iron corrosion, Appl. Catal., B, 104 (2011) 185–192.

[23] T. Kohn, W.A. Arnold, A.L. Roberts, Reactivity of substituted benzotrichlorides toward granular iron, Cr(II), and an iron(II) porphyrin: a correlation analysis, Environ. Sci. Technol., 40 (2006) 4253–4260.

[24] V. Janda, P. Vasek, J. Bizova, Z. Belohlav, Kinetic models for volatile chlorinated hydrocarbons removal by zero-valent iron, Chemosphere, 54 (2004) 917–925.

[25] C. Lee, D.L. Sedlak, Enhanced formation of oxidants from bimetallic nickel−iron nanoparticles in the presence of oxygen, Environ. Sci. Technol., 42 (2008) 8528–8533.

[26] K.S. Wang, C.L. Lin, M.C. Wei, H.H. Liang, H.C. Li, C.H. Chang, S.H. Chang, Effects of dissolved oxygen on dye removal by zero-valent iron, J. Hazard. Mater., 182 (2010) 886–895.